

Dissimilar Material Joints With and Without Free-edge Stress Singularities: Part I. A Biologically Inspired Design

by L.R. Xu, H. Kuai and S. Sengupta

ABSTRACT—An integrated experimental and numerical investigation was conducted for removing the free-edge stress singularities in dissimilar material joints. A convex interface/joint design, inspired by the shape and mechanics of trees, will result in reduced stress singularities at bi-material corners for most engineering material combinations. *In situ* photoelasticity experiments on convex polycarbonate–aluminum joints showed that the free-edge stress singularity was successfully removed. As a result, the new design not only improves the static load transfer capacity of dissimilar material joints, but also yields more reasonable interfacial tensile strength evaluation. For convex polycarbonate–aluminum and poly(methyl methacrylate)–aluminum joint specimens, the ultimate tensile load increased up to 81% while the total material volume was reduced by at least 15% over that of traditional butt-joint specimens with severe free-edge stress singularities.

KEY WORDS—Bonding, dissimilar materials, interface, photoelasticity, stress singularities

Introduction

Dissimilar material interfaces/joints can be found in numerous modern engineering and science fields, for example, adhesive bonded interfaces of two dissimilar materials, fiber/matrix interfaces of composite materials, thin film/substrate interfaces in microelectromechanical systems (MEMS), to name a few. One major research effort in interface studies has been the interfacial strength evaluation of dissimilar materials.^{1–7} Meanwhile, numerous studies have shown that failure often occurs along the interface/joint between two types of material with high property mismatch (e.g., free-edge delamination in composite laminates and debonding between thin films/substrates), and that improving the interfacial properties (especially reducing the interfacial stress level) can modify overall material/structural behavior.^{8–10} Recent efforts also reveal that the chemical and mechanical aspects of interfacial bonding are essential for nanostructured material development.¹¹ Indeed, interfacial bonding between the nanoscale reinforcement and the

matrix is one of the most important research subjects in the development of nanocomposite materials.¹²

However, macroscale interfacial strength measurement is still a major challenge due to the stress singularity problem,^{13–15} i.e., the theoretical stress will be infinite at the free edges. On the other hand, modern numerical tools, such as the cohesive element method, have an urgent need for interfacial strengths and toughnesses as important data input. Hence, it is necessary to develop reliable quantitative measurements in order to characterize interfacial properties. As interfacial mechanical properties are intrinsic in nature, they are solely determined by the atomic structure and chemistry of the interfacial region.¹⁶ However, the interfacial strength based on current measurements is not a material constant due to the free-edge stress singularity, according to some recent investigations.¹³ Recently, Tandon et al.¹⁴ have proposed a novel specimen design to measure the interfacial strength of fiber/matrix bonding. The key issue in measuring intrinsic interfacial strengths is the creation of a uniform interfacial stress state. So, the first important step for intrinsic interfacial strength measurement is the elimination of stress singularities. Actually, elimination of stress singularities is also very valuable for structural/material joints subjected to fatigue and dynamic loading, since failure often occurs from the bi-material free edge due to stress singularities.^{7,17}

The objectives of this investigation are to propose novel specimen designs to remove the stress singularity, and therefore to provide reasonable interfacial strength measurements and suppress edge debonding of dissimilar material joints. We review the origin of stress singularities, and we propose a general solution inspired by the mechanics during formation of trees, a biologically inspired design.¹⁸ Typical metal/polymer joints will be selected for demonstration of the proposed new design through an *in situ* photoelasticity experiment.

Theoretical Background

Free-edge Stress Singularities in Dissimilar Material Interfaces/joints

As illustrated in Fig. 1(a), a butt-joint specimen was used to demonstrate the free-edge stress singularity in steel 4340 and Plexiglas (poly(methyl methacrylate) (PMMA)) joints.¹⁹ Significant stress concentrations were found at the bi-material corners using the coherent gradient sensing (CGS) technique, which was developed by Tippur et al.²⁰ for full-field mechanical–optical measurements. The CGS fringe patterns

L.R. Xu (SEM Member; l.roy.xu@vanderbilt.edu) is an Assistant Professor, and H. Kuai and S. Sengupta are Graduate Research Assistants, Department of Civil and Environmental Engineering, VU Station B 351831, 2301 Vanderbilt Place, Vanderbilt University, Nashville, TN 37235, USA.

Original manuscript submitted: December 30, 2003.

Final manuscript received: September 14, 2004.

DOI: 10.1177/0014485104049399

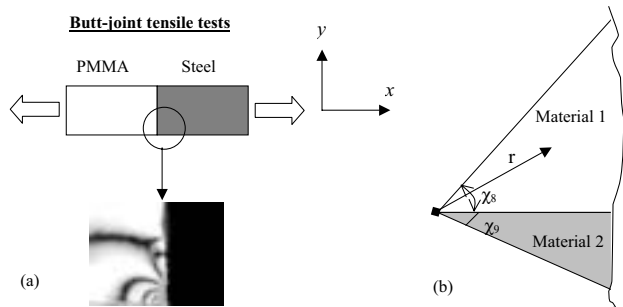


Fig. 1—(a) CGS photograph showing a strong stress concentration (associated with fringe pattern concentrations) at the free edges of a bonded metal and polymer subjected to tensile load.¹⁹ (b) Angular definition of a bi-material wedge

correspond to the gradients of $\sigma_{xx} + \sigma_{yy}$. It is indeed this concentration/singularity that leads to free-edge debonding, especially when the joint is subjected to dynamic and fatigue loading.

For some specific bi-material corners or edges, Williams,²¹ Bogy,²² Hein and Erdogan,²³ Munz and Yang,²⁴ Pageau et al.,²⁵ Akisanya and Meng,²⁶ Klingbeil and Beuth,²⁷ and Labossiere et al.,²⁸ to name a few, have shown that stress singularities exist. The asymptotic stress field of a bi-material corner can be expressed by

$$\sigma_{ij}(r, \theta) = \sum_{k=0}^N r^{-\lambda_k} K_k f_{ijk}(\theta) \quad (i, j = 1, 2, 3) \quad (1)$$

where $f_{ijk}(\theta)$ is an angular function and K_k is also known as the “stress intensity factor”. The fracture mechanics terminology “stress intensity factor” is used in interfacial mechanics to characterize a similar stress singularity problem. It should be noticed that, for an interfacial fracture problem (assuming initial debonding), the stress singularity at a crack tip is intrinsic and cannot be removed. However, the stress singularity in an interfacial strength investigation (assuming perfect bonding) can be removed through appropriate designs; a key issue in this investigation. The stress singularity order λ may be real or complex. Here, we did not use other singularity order forms such as $\lambda - 1$, because the value of λ can be easily ascertained by the readers. Also, it is conveniently compared to the singularity order -0.5 of a crack based on linear elastic fracture mechanics (LEFM). Hence, the theoretical stress values will become infinite as r (defined in Fig. 1(b)) approaches zero, if λ has a positive real part. This leads to a problem referred to as the “stress singularity problem”. It is the presence of this stress singularity that leads to erroneous results in current interfacial strength measurements, besides being responsible for free-edge debonding or delamination in dissimilar material joints. However, if λ has a non-positive real part, then the stress singularity disappears. Our major research effort is focused on producing a non-positive real part for λ using a new interfacial design approach.

Bogy²² found that the stress singularity was purely determined by the material property mismatch and two joint angles of the bi-material corner θ_1, θ_2 (defined in Fig. 1(b)). Generally, the material property mismatch can be expressed in terms of the Dundurs parameters α and β , which are two

non-dimensional parameters computed from the elastic constants of two bonded materials:²⁹

$$\alpha = \frac{\mu_1 m_2 - \mu_2 m_1}{\mu_1 m_2 + \mu_2 m_1}$$

$$\beta = \frac{\mu_1(m_2 - 2) - \mu_2(m_1 - 2)}{\mu_1 m_2 + \mu_2 m_1} \quad (2)$$

Here, μ_1 is the shear modulus of material 1, μ_2 is the shear modulus of material 2, $m = 4(1 - \nu)$ for plane strain, ν is the Poisson ratio, and $m = 4/(1 + \nu)$ for generalized plane stress.

The stress singularity order is related to material and geometric parameters, and is determined by a characteristic equation of coefficients $A(\theta_1, \theta_2, p)$ through $F(\theta_1, \theta_2, p)$:

$$f(\theta_1, \theta_2, \alpha, \beta, p) = A\beta^2 + 2B\alpha\beta + C\alpha^2 + 2D\beta + 2E\alpha + F = 0, \quad (3)$$

where $p = 1 - \lambda$. A, B, C, D, E , and F have been defined by Bogy.²² Therefore, our basic idea is to vary these four independent parameters ($\theta_1, \theta_2, \alpha, \beta$) in order to obtain a negative real part of the stress singularity order λ . Thus, the stress distribution close to the free edge will be smooth.

Convex Interfacial Joints for Uniform Interfacial Stress Distribution

The first step to establish a uniform stress state at the interface is to reduce or eliminate the stress singularity at the bi-material edge. Mattheck³⁰ analyzed an interesting problem of a tree/steel railing interface, as illustrated in Fig. 2, where it may be seen that the railing predates the tree. Initially, the intrusion caused by the railing gives rise to high stresses in the tree trunk. The natural instinct of the tree is then to grow around the railing in a convex manner and thereby to reduce the stress. This biological explanation was verified by Mattheck’s finite-element analysis (FEA) where he showed that for a total joining angle $\theta_1 + \theta_2 = 270^\circ$, the Mises stress has a very high concentration value at the joint corner. A better design is the naturally formed convex shape, which corresponds to the optimized case shown in Fig. 2. As recently noticed by Mohammed and Liechti,³¹ an appropriate joining angle design at the bi-material edge is a possible approach to reduce the stress singularity. This is clearly indicated in the determinant $f(\theta_1, \theta_2, \alpha, \beta, p)$ introduced by Bogy.²² Since we can choose appropriate angular combinations according to different material combinations, it is possible to obtain a negative or zero $\text{Re}[\lambda]$. Interpreted, this means that the degree of singularity can be reduced or removed. From this step, we can determine two joint angles.

After several numerical case studies, we have chosen an interfacial design with two joint angles, $\theta_1 = 65^\circ$ and $\theta_2 = 45^\circ$, and we assume that material 1 is a typical hard material and that material 2 is a soft material. Thus, there will be no stress singularity for a wide range of current engineering materials (the small deviation of this pair of joint angles will not change the result).³² This result is illustrated in Fig. 3 within the entire possible range of two Dundurs parameters.⁸ We can see that for this specific pair of joint angles, the stress singularity is limited to a very small zone near $\alpha \cong 1$. These extreme material joint combinations are

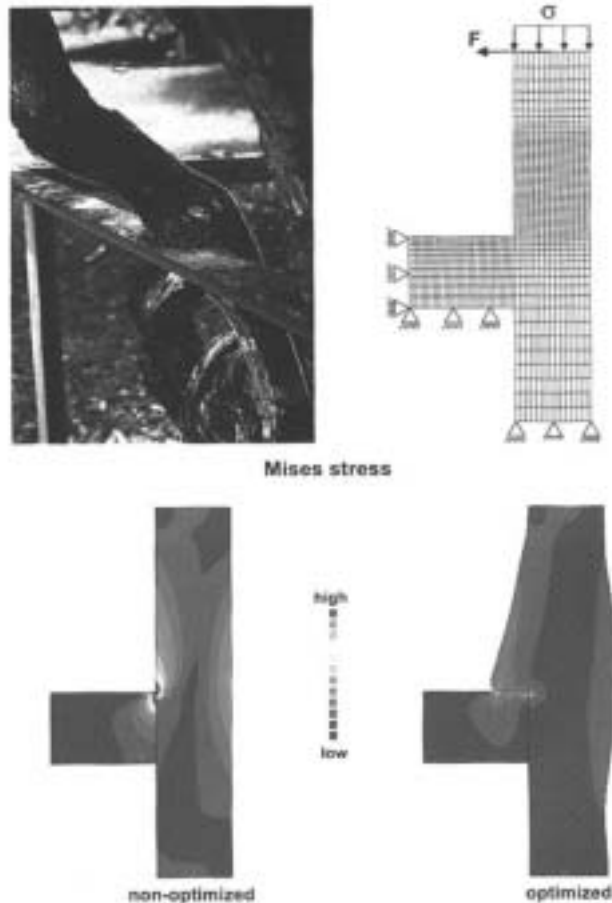


Fig. 2—Finite-element stress analysis and corner optimization of a tree–steel railing interface/joint.³⁰ The natural convex joint shows no stress concentrations/ singularities

quite rare in engineering applications since they represent extremely high mismatch in Young’s moduli. Recent examples include nanotube/nanofiber reinforced polymer composites since the Young’s modulus of carbon nanotubes is as high as 1000 GPa. Xu et al.¹² have reported a value of $\alpha \cong 0.99$ for a new nanofiber/epoxy composite. To demonstrate the zero stress singularity of proposed convex interfacial joints, an *in situ* experimental validation is necessary.

Experimental Investigation

The major purpose of the experimental study is to verify that the new convex joints are effective in removing stress singularities. *In situ* photoelasticity experiments will be employed in conjunction with FEA in Part II of this investigation.³²

Specimen Design and Preparation

Two types of specimen were designed and prepared for comparison, as seen in Fig. 4. The straight edge specimen is the baseline for comparisons. All the designs were analyzed using the commercial finite-element method (FEM) software ANSYS.³² Besides the joining angles, other parameters of the convex specimens, such as the convex extension distance and the material elastic properties, were varied in the simu-

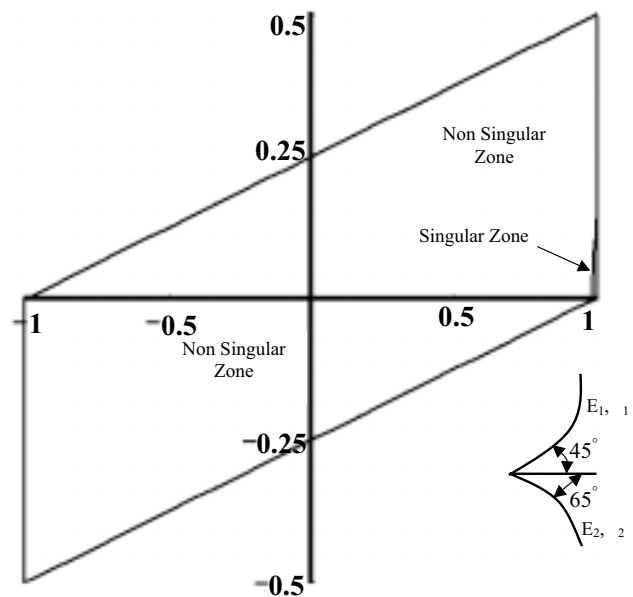


Fig. 3—Stress singularity order λ as a function of two Dundurs parameters for a proposed pair of joint angles (45° and 65° for soft and hard materials, respectively). A very small singular zone implies the given pair of joint angles is applicable for a wide range of engineering material combinations

lations. The test materials were PMMA, polycarbonate, and aluminum. Two groups of material combinations were tested: (i) PMMA and aluminum; (ii) polycarbonate and aluminum. The nominal specimen thickness was 6.35 mm (0.25 inch). In order to obtain more fringes in the photoelasticity experiments, thick specimens (9.35 mm) of polycarbonate and aluminum were used. A commercial epoxy (Weld-on 10, Meyer Plastics Inc., Santa Ana, CA) was used as the bonding agent. The reason to choose this particular adhesive is that its properties are very close to those of PMMA or polycarbonate.²⁰ Hence, the possible involvement of a third material in a typical bi-material problem was removed. The adhesive had two components, A and B. They were mixed before bonding and cured at room temperature for at least 4 h. After 24 or 48 h, it reached the design strength. Before the adhesive bonding, bonding areas were sand blasted and cleaned using acetone. A special fixture was designed to bond these specimens. The alignment of these specimens was carefully examined during the bonding process.

Experimental Setup

A mechanical–optical system was used to record the *in situ* fringe pattern development during loading process, as shown in Fig. 5. The whole setup consists of an optical system, a mechanical testing system, and an imaging system. The mechanical testing system included an MTS 810 test machine. The optical system was utilized to capture the *in situ* fringe pattern development (related to in-plane stress development) during tests. A laser beam was transmitted through the transparent polymeric specimen, and the resulting fringe pattern was recorded by a camera. Photoelasticity experiments were performed for polycarbonate specimens. The isochromatic

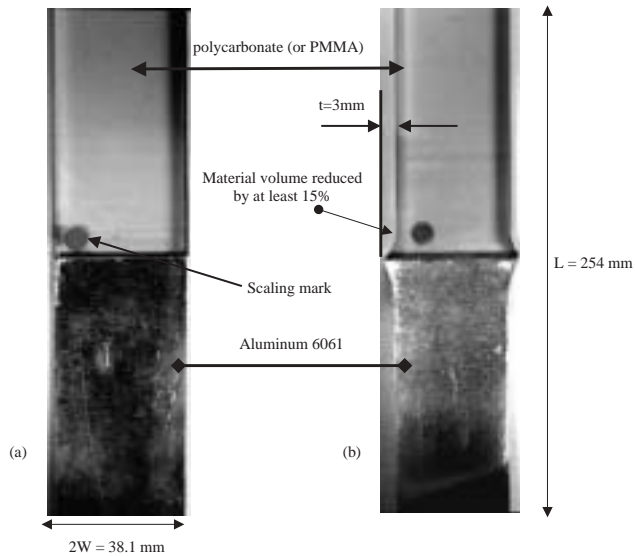


Fig. 4—Pictures of two types of aluminum–polycarbonate joint specimens with the same bonding area but different joint angles: (a) straight edges (baseline); (b) shaped edges with least stress singularities

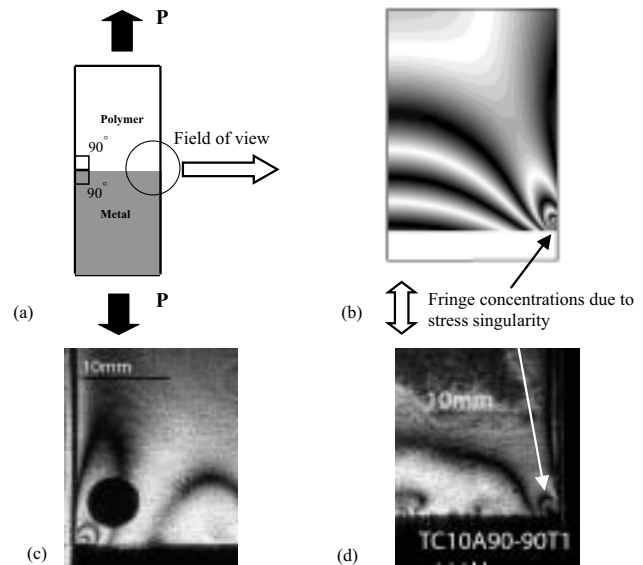


Fig. 6—Comparison of numerical and experimental photoelasticity patterns for different PC/Al joints with straight edges under the same applied load, $P = 1000\text{ N}$

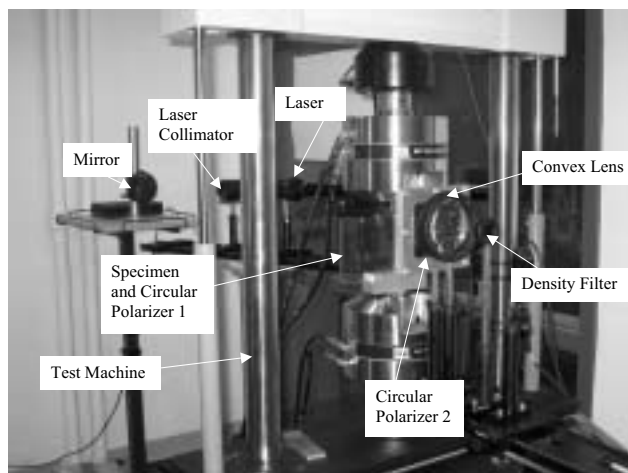


Fig. 5—Experimental setup of a mechanical–optical system to record *in situ* stress development during loading process

fringe patterns observed are the contours of the maximum in-plane shear stress

$$\tau_{max} = (\sigma_1 - \sigma_2)/2 = \frac{Nf\sigma}{2h}, \quad (4)$$

where σ_1 and σ_2 are in-plane principal stresses, N is the fringe order, $f\sigma$ is the stress-fringe constant, and h is the specimen thickness.³³

The optical system included an He–Ne laser source (17 mW), a laser collimator, a reflection mirror, and two circular polarizer sheets for photoelasticity experiments. The function of the collimator was to provide a large and collimated laser beam (diameter 50 mm) since the field of view of our specimens was at least 10 mm. The purpose of the mirror was to adjust the laser beam to a desired position for a specific

experiment. The imaging system included a high-resolution digital camera to capture the fringe development, and a density filter in front of the camera to reduce the laser intensity since the laser beam entered the camera directly. Because the laser beam diameter was about 50 mm, a convex lens (focal length 150 mm) was added to the system to record the whole image. An important issue in obtaining good-quality photos is that the digital camera must be focused at infinity, and that the distance between the convex lens and the specimen should be slightly larger than the focal length of the convex lens.

Results and Discussion

Straight-edge Specimens With Severe Stress Singularities

An aluminum–polycarbonate interface with a pair of joining angles of 90° – 90° (both aluminum and polycarbonate parts are rectangular shaped) was chosen as the baseline for comparison and the results are illustrated in Fig. 6. FEA showed that the value of stress singularity order λ ranged from 0.216 to 0.223, based on interfacial normal and shear stress distributions.³² The analytical value of λ based on eqs (3) and (4) is 0.225 for this specific material and angle joint. Figure 6 is a direct comparison of numerical and experimental fringe patterns, and bears the most conclusive testimony to the stress singularity at the free edges of dissimilar material joints. After the fringe order N was computed at every node using eq (4), a corresponding gray-scale value was calculated by associating a gray-scale value of 255 with full-fringe orders (e.g., 0, 1, 2, etc.) and a value of 0 with half-fringe orders (e.g., 0.5, 1.5, 2.5, etc.). Tecplot 9.2 plotting software was then used to plot these gray-scale values, and the numerical fringe patterns shown in Fig. 6 were generated for stress field visualization and comparison with experimental results.

It is rather interesting to note that a clear fringe concentration originates at the interface corner of the straight-edged

specimen, as shown in Fig. 6. This type of fringe concentration is a result of the free-edge stress singularity and is very similar to the fringe concentration caused by a bi-material interfacial crack.⁷ We notice that the stress singularity order for Al/PC joints is around -0.2 and can be eliminated, but for interfacial cracks the stress singularity order is $-0.5 + i\epsilon$ (see Rice³⁴) and is intrinsic. A direct comparison of the numerical fringe pattern (Fig. 6(b)) and the experimental pattern (Figs. 6(c) and (d)) of the different specimens subjected to the same applied load of 1000 N verifies the existence of stress singularity at the free edge. In the next section, we demonstrate that our simple joint angle design can remove this type of stress singularity/concentration.

Convex Joints Without Stress Singularities

The accumulation of fringes at the bimaterial interfacial corner, seen in the straight-edged specimens, completely disappeared in the photoelasticity fringe patterns of the shaped specimen as seen in Fig. 7. For different load levels from 500 to 1500 N, no fringe pattern concentration was observed in a convex joint, as seen in Figs. 7(b), (d), and (f). The numerical fringe pattern (applied load 1000 N) also validates this result, as shown in Fig. 7(c). Fig. 7(e) is another picture from a different specimen with the same Al/PC interface under the same load of 1000 N. The highest fringe order actually went up to 23.5 for the straight-edged specimens, whereas the highest fringe order in the shaped specimens under the same 500 N applied load was only 6.5 (see Xu and Sengupta³²). This is a clear indication that the stress intensity has decreased by several orders in the proposed convex joint. It is noticed that the higher fringe orders signifying larger stress intensity move away from the interface towards the polycarbonate curved edge. This stress redistribution is indeed very important in interfacial joint designs since the bonding strength of the interface is generally lower than that of the bulk material (adherend).^{35,36} For example, the tensile strength of bulk polycarbonate is at least 60 MPa, whereas the nominal interfacial tensile strength of PC/Al joints in this investigation is around 5–6 MPa.

More interesting results are revealed using FEA:³² the influence of the convex extension distance t on the normal stress distribution at the interface. Four cases have been examined: $t = 0$ (straight-edged or baseline specimens), 0.5, 1.0, and 3.0 mm (shaped specimens). For zero extension distance, i.e., straight-edged specimens, a prominent stress singularity was seen at the intersection of the bimaterial interface. However, for increasing extension distances, the interfacial normal stress has a finite value at the interface corner and the stress distribution is seen to smoothen out over the interface to a uniform value. From this analysis, we find that the stress singularity has been successfully removed. Since the stress singularity directly contributes to the free-edge delamination or debonding, this results in a corresponding increase of the load transfer capability of the new joint.

Obviously, since we have reduced the maximum interfacial stress level in shaped specimens and moved the maximum stress location away from the interface, we expect to push the envelope of failure load for the proposed convex joints subjected to in-plane load. The increase in tensile load capacity of the convex interfacial joints of aluminum–polycarbonate and aluminum–PMMA combinations is recorded in Tables 1 and 2, and is illustrated in Fig. 8. All shaped specimens showed a marked increase in nominal tensile strengths (ul-

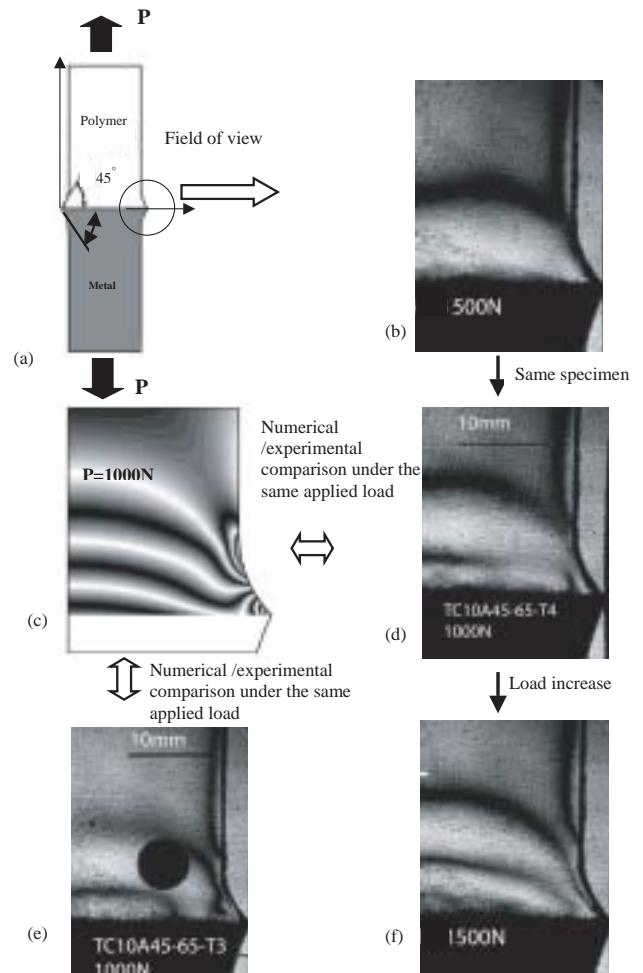


Fig. 7—Development of photoelasticity patterns for load (b) $P = 500$ N, (d) $P = 1000$ N, and (f) $P = 1500$ N in a typical PC/Al joint with shaped edges. (c) is a numerical photoelasticity pattern under $P = 1000$ N and (e) is an experimental pattern from a different specimen

imate load/interface area) over that of straight-edged specimens. The proposed convex joint is indeed very efficient since the tensile load capacity has increased up to 81% while the total material volume has reduced by at least 15%. The influence of specimen thickness has also been considered. It was noticed that thicker specimens with a thickness of 9 mm showed less tensile strength increase than thin specimens with a thickness of 6 mm. This phenomenon raises an interesting question for reasonable interfacial strength and fracture toughness characterizations.

Comparison of Traditional Strength and Interfacial Strength Measurements

The strength definition of a homogeneous material is quite straightforward: it is the failure stress of the specimen with a uniform stress state across the cross-section, as illustrated in Fig. 9(a). Since the final failure of the material is associated with the initial defect distribution at the cross-section, specimens with different sizes will yield different strength data (e.g., Weibull strength distribution) although there is no length-scale involved in the stress distribution of these

TABLE 1—TENSILE TEST DATA OF PMMA—ALUMINUM JOINTS

Specimen Code	Joint Angles (PMMA—A1)	Tensile Strength (MPa)	Change of Strength	Standard Deviation (MPa)	Specimen Thickness (mm)
TP10A90-90	90°–90° (baseline)	5.9	0%	1.2	6
TP10A45-65	45°–65°	10.1	+71%	1.4	6

TABLE 2—TENSILE TEST DATA OF POLYCARBONATE—ALUMINUM JOINTS WITH DIFFERENT SPECIMEN THICKNESSES

Specimen Code	Joint Angles (PC—A1)	Tensile Strength (MPa)	Change of Strength	Standard Deviation (MPa)	Specimen Thickness (mm)
TC10A90-90	90°–90° (baseline)	2.6	0%	0.7	6
TC10A45-65	45°–65°	4.7	+81%	2.0	6
TC10A90-90T (thick specimens)	90°–90° (baseline)	5.3	0%	1.4	9
TC10A45-65T (thick specimens)	45°–65°	5.6	+6%	1.5	9

specimens. This phenomenon may be defined as “the material size effect”. As discussed before, interfacial strength measurement is quite complicated because of the possible stress singularity and highly non-uniform interfacial stress distributions, as shown in Fig. 9(b). Therefore, any interfacial strength experiment must be carefully examined, otherwise it may yield meaningless data.

For a tensile specimen constituted of the same material illustrated in Fig. 9(a), the normal tensile stress at any cross-section is always uniform. Although the size effect of this type of specimen still exists due to initial material defects, specimens made of the same material have no length-scale involved in terms of their stress states. However, for a tensile specimen fabricated from two dissimilar materials with straight free edges (a typical example of current material test standards) shown in Fig. 9(b), the normal stress distribution across the interface is not uniform, according to previous theoretical analysis and experimental verification. The asymptotic stress field at the bi-material corner is related to a significant length-scale $r^{-\lambda}$. Obviously, this type of specimen will provide data with a strong size effect in the context of mechanical behavior. Moreover, the mechanics size effect (related to the free-edge stress singularity) will be coupled with the material size effect, and thus lead to complexities in measurement data, which cannot be treated as intrinsic material properties. Therefore, the measured nominal interfacial strengths based on current test standards cannot be used in mechanics predictions because the interfacial properties obtained from laboratory tests are quite different from the real values of structures in service. For example, the two types of PMMA/Al joint specimens with the same material interface and cross-section area as seen in Table 1 and Fig. 9(a) should yield the same tensile strength if the interfacial strength is indeed a material constant. However, in actuality, the difference of these two nominal tensile strengths is 71%.

Due to the stress singularity at the free edge, failure of the bi-material specimen always initiated at the specimen edge rather than at the center in our previous experiments.¹⁹ Hence, the interfacial strength from the current measurement stan-

dard is directly related to the singular stress state and initial defects at the edge only, rather than to a uniform stress state and all initial material defects at the whole interface. In order to measure an intrinsic interfacial strength, a uniform stress distribution across the interface should be created. Thus, all initial defects will have equal probability of leading to final failure (breaking the interface). This type of strength data should be very close to intrinsic tensile strengths when the interface is loaded to failure. It is naturally expected that the convex joint specimen should yield a reasonable interfacial tensile strength value since the interfacial normal stress is quite uniform. The above strength analysis is based on the assumption of a perfectly bonded interface. However, during the bonding process, initial debonding or defects always exist. Figure 10 shows that the initial defects became macroscale interfacial cracks (at least 1–2 mm in crack length) in both baseline and shaped specimens before final failure. This raises another important issue of interfacial fracture.

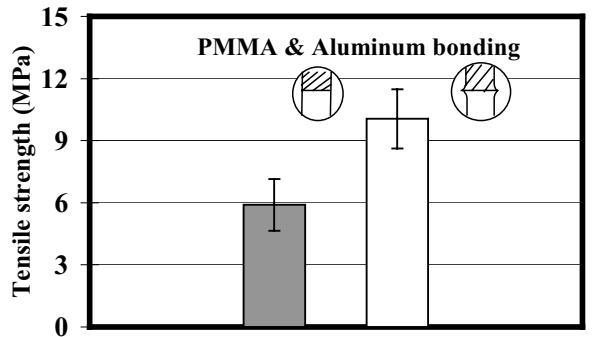
Role of Interface Strength in Interfacial Fracture Investigation

The intrinsic interfacial strength (perfect interfacial bonding/no cracks) is also necessary to solve an interfacial fracture mechanics problem. Besides the interfacial strength, another important parameter for interfacial mechanical property characterization is the interfacial fracture toughness/stress intensity factor. In general, an interfacial crack between two dissimilar materials can be characterized by a complex interfacial stress intensity factor, $K = K_1 + iK_2$. The stress field can be expressed as^{8,34}

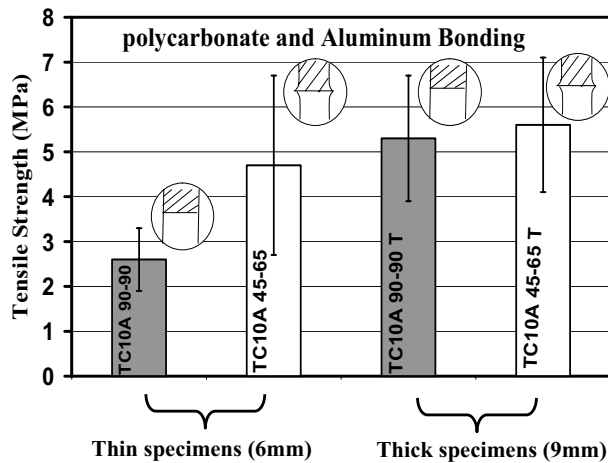
$$\sigma_{yy} + i\sigma_{xy} = -\frac{1}{\sqrt{2\pi}} K r^{-1/2+i\varepsilon} \quad (5)$$

where the oscillatory index ε depends on only one of the Dundurs parameters, β :

$$\varepsilon = \frac{1}{2\pi} \ln \left(\frac{1-\beta}{1+\beta} \right). \quad (6)$$



(a)



(b)

Fig. 8—Bar charts depicting comparison of measured nominal tensile strengths for baseline and shaped specimens: (a) Al/PMMA joints; (b) Al/PC joints. Significant ultimate tensile load capacity was achieved in shaped specimens with least stress singularities

Here, we notice that the stress singularity order ($-1/2 + i\epsilon$) at a crack tip is intrinsic and cannot be removed, while the stress singularity from free edges can be removed through appropriate designs in this investigation. For homogeneous materials with no material property mismatch, the two Dundurs parameters, α and β , are zero. So K_1 and K_2 can be interpreted as the classical mode I and II stress intensity factors. Both interfacial strength and fracture toughness are necessary to characterize an interfacial fracture problem. This can be clearly explained using an important numerical tool: the cohesive crack model. In order to simulate an interfacial crack, three parameters including the interfacial strength and cohesive energy, etc., are needed as data input.^{9,37,38} The cohesive energy (fracture toughness) alone is not enough for a cohesive crack model.

Conclusions

Convex interfacial joints prove to be quite effective in eliminating free-edge stress singularity in dissimilar materi-

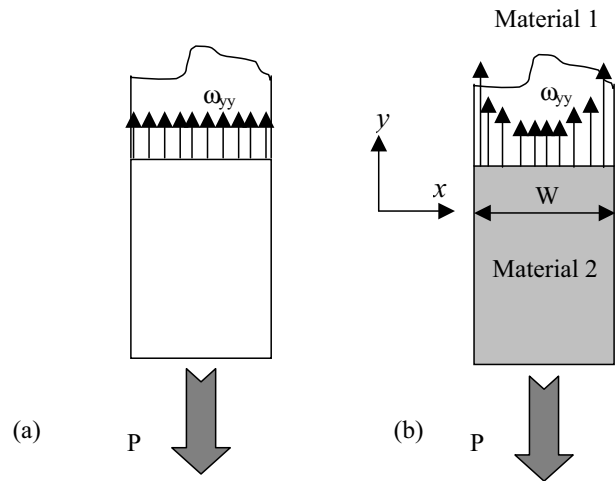


Fig. 9—Normal stress distributions of typical tensile specimens constituted of (a) same material and (b) dissimilar materials

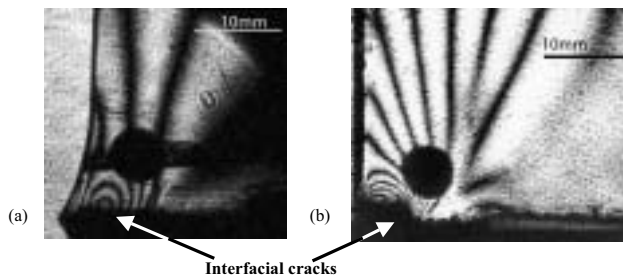


Fig. 10—Interfacial cracks originated from initial defects before the final tensile failure in (a) shaped specimens and (b) straight-edge specimens

als and structures. An integrated experimental and numerical investigation shows that a specific convex interfacial joint not only produces reasonable interfacial strength measurement, but also improves the ultimate tensile load capacity of hybrid joints. For convex polycarbonate–aluminum joint specimens, the tensile load capacity increased up to 81% while the material volume reduced by at least 15% over that of traditional butt-joint specimens with severe free-edge stress singularities. Indeed, our new solution to a long-term problem in mechanics of materials (free-edge stress singularities) was inspired from the mechanics principles underlying tree shapes. This investigation just presents a simple example of biologically inspired design to enhance scientific and technological understanding, i.e., nature may have provided efficient solutions for certain difficult technological problems.

Acknowledgments

LRX gratefully acknowledges the support from the Office of Naval Research Young Investigator Award (N00014-03-1-0505, Dr Roshdy G. S. Barsoum, Program Officer), and the National Science Foundation, Surface Engineering

and Materials Design Program (CMS-0409665, Dr Yip-Wah Chung, Program Director). Helpful discussions with Professor P. Joseph, Professor A.J. Rosakis, and Dr. O. Samudrala are appreciated.

References

1. Drzal, L.T., "Fiber Matrix Interphase Structure and Its Effect on Adhesion and Composite Mechanical Properties," *Controlling Interphases in Composite Materials*, H. Ishida, editor, Elsevier, Amsterdam, 309–319 (1990).
2. Gupta, V., Yuan, J., and Pronin, A., "Recent Developments in the Laser Spallation Technique to Measure the Interface Strength and Its Relationship to Interface Toughness with Applications to Metal/Ceramic, Ceramic/Ceramic and Ceramic/Polymer Interfaces," *Journal of Adhesion Science and Technology*, **8**, 713–747 (1994).
3. Lara-Curzio, E., Ferber, M.K., Besmann, T.M., Rebillat, F., and Lammon, J., "Fiber-matrix Bond Strength, Fiber Frictional Sliding and the Macroscopic Tensile Behavior of a 2D SiC/SiC Composite with Tailored Interfaces," *Ceramics Engineering and Science*, **15**, 597–612 (1995).
4. Rabin, B.H., Williamson, R.L., Bruck, H.A., Wang, X.-L., Watkins, T.R., Feng, Y.-Z., and Clarke, D.R., "Residual Strains in an Al203–Ni Joint Bonded With a Composite Interlayer: Experimental Measurements and FEM Analyses," *Journal of American Ceramics Society*, **81**, 1541–1549 (1998).
5. Lin, G., Geubelle, P.H., and Sottos, N.R., "Simulation of Fiber Debonding With Friction in a Model Composite Push-out Test," *International Journal of Solids and Structures*, **38**, 8547–8562 (2001).
6. Zhou, X.-F., Wagner, H.D., and Nutt, S.R., "Interfacial Properties of Polymer Composites Measured by Push-out and Fragmentation Tests," *Composites Part A*, **32**, 1543–1551 (2001).
7. Xu, L.R. and Rosakis, A.J., "Impact Failure Characteristics in Sandwich Structures: Part II. Effects of Impact Speed and Interfacial Strength," *International Journal of Solids and Structures*, **39**, 4237–4248 (2002).
8. Hutchinson, J.W. and Suo, Z., "Mixed-mode Cracking in Layered Materials," *Advances in Applied Mechanics*, **29**, 63–191 (1992).
9. Needleman, A. and Rosakis, A.J., "The Effect of Bond Strength and Loading Rate on the Conditions Governing the Attainment of Intersonic Crack Growth Along Interfaces," *Journal of Mechanics and Physics of Solids*, **47**, 2411–2449 (1999).
10. Xu, L.R., Huang, Y.Y., and Rosakis, A.J., "Dynamic Crack Deflection and Penetration at Interfaces in Homogeneous Materials: Experimental Studies and Model Predictions," *Journal of Mechanics and Physics of Solids*, **51**, 461–486 (2003).
11. Thostenson, E.T., Li, W., Wang, D., Ren, Z., and Chou, T., "Interfacial Characterization of Carbon Nanotube-modified Graphite Fiber Composites," *Proceedings of the 16th American Society of Composites Technical Conference*, Blacksburg, VA, CRC Press, Boca Raton (2001).
12. Xu, L.R., Bhamidipati, V., Zhong, W.-H., Li, J., Lukehart, C.M., Lara-Curzio, E., Liu, K.C., and Lance, M.J., "Mechanical Property Characterization of a Polymeric Nanocomposite Reinforced by Graphitic Nanofibers With Reactive Linkers," *Journal of Composite Materials*, **38**, 1563–1582 (2004).
13. Reedy, E.D. Jr and Guess, T.R., "Comparison of Butt Tensile Strength Data with Interface Corner Stress Intensity Factor Prediction," *International Journal of Solids and Structures*, **30**, 2929–2936 (1993).
14. Tandon, G.P., Kim, R.Y., Warriar, S.G., and Majumdar, B.S., "Influence of Free Edge and Corner Singularities on Interfacial Normal Strength: Application in Model Unidirectional Composites," *Composites, Part B: Engineering*, **30**, 115–134 (1999).
15. Akisanya, A.R. and Fleck, N.A., "Interfacial Cracking from the Free Edge of a Long Bi-material Strip," *International Journal of Solids and Structures*, **34**, 1645–1665 (1997).
16. Swadener, J.G., Liechti, K.M., and de Lozanne, A.L., "The Intrinsic Toughness and Adhesion of a Glass Epoxy Interface," *Journal of the Mechanics and Physics of Solids*, **47**, 223–258 (1999).
17. Pelegri, A.A., Kardomateas, G.A., and Malik, B.U., "The Fatigue Growth of Internal Delaminations Under Compressive Loading in Cross Ply Composite Plates," *Composite Materials: Fatigue and Fracture*, ASTM STP 1285, E.A. Armanios, editor, 146–163 (1997).
18. Bruck, H.A., Evans, J.J., and Peterson, M.L., "The Role of Mechanics in Biological and Biologically Inspired Materials," *EXPERIMENTAL MECHANICS*, **42**, 361–371 (2002).
19. Xu, L.R., Rosakis, A.J., and Samudrala, O., "Measurements of Adhesive Tensile and Shear Strengths With the Aid of Two Optical Techniques," *Proceedings of the Society of Experimental Mechanics Annual Conference*, San Diego, CA (2002).
20. Tippur, H.V., Krishnaswamy, S., and Rosakis, A.J., "A Coherent Gradient Sensor for Crack Tip Deformation Measurements: Analysis and Experimental Results," *International Journal of Fracture*, **48**, 193–204 (1991).
21. Williams, M.L., "Stress Singularities Resulting From Various Boundary Conditions in Angular Corners of Plates in Extension," *Journal of Applied Mechanics*, **19**, 526–528 (1952).
22. Bogy, D.B., "Two Edge-bonded Elastic Wedges of Different Materials and Wedge Angles Under Surface Traction," *Journal of Applied Mechanics*, **38**, 377–386 (1971).
23. Hein, V.L. and Erdogan, F., "Stress Singularities in a Two-material Wedge," *International Journal of Fracture Mechanics*, **7**, 317–330 (1971).
24. Munz, D. and Yang, Y.Y., "Stresses Near the Edge of Bonded Dissimilar Materials Described by Two Stress Intensity Factors," *International Journal of Fracture*, **60**, 169–177 (1993).
25. Pageau, S.S., Gadi, K.S., Biggers, S.B., and Joseph, P.F., "Standardized Complex and Logarithmic Eigensolutions for n-material Wedges and Junctions," *International Journal of Fracture*, **77**, 51–76 (1996).
26. Akisanya, A.R. and Meng, C.S., "Initiation of Fracture at the Interface Corner of Bi-material Joints," *Journal of the Mechanics and Physics of Solids*, **51**, 27–46 (2003).
27. Klingbeil, N.W. and Beuth, J.L., "On the Design of Debond-resistant Bi-materials, Part I. Free-edge Singularity Approach," *Engineering Fracture Mechanics*, **66**, 93–110 (2000).
28. Labossiere, P.E.W., Dunn, M.L., and Cunningham, S.J., "Application of Bi-material Interface Corner Failure Mechanics to Silicon/Glass Anodic Bonds," *Journal of the Mechanics and Physics of Solids*, **50**, 405–433 (2002).
29. Dundurs, J., "Discussion of Edge-bonded Dissimilar Orthogonal Elastic Wedges Under Normal and Shear Loading by Bogy D.B.," *ASME Journal of Applied Mechanics*, **36**, 650–652 (1969).
30. Mattheck, C., *Design in Nature: Learning from Trees*, Springer-Verlag, New York (1998).
31. Mohammed, I. and Liechti, K.M., "The Effect of Corner Angles in Bi-material Structures," *International Journal of Solids and Structures*, **38**, 4375–4394 (2001).
32. Xu, L.R. and Sengupta, S., "Dissimilar Material Joints With and Without Free-edge Stress Singularities: Part II. An Integrated Numerical Analysis," *EXPERIMENTAL MECHANICS*, **44** (6), 616–621 (2004).
33. Kobayashi, A.S., editor, *Handbook on Experimental Mechanics*, Society for Experimental Mechanics, Prentice-Hall, Englewood Cliffs, NJ (1987).
34. Rice, J.R., "Elastic Fracture Mechanics Concepts for Interfacial Cracks," *Journal of Applied Mechanics*, **55**, 98–103 (1988).
35. Xu, L.R., Sengupta, S., and Kuai, H., "An Experimental and Numerical Investigation on Adhesive Bonding Strengths of Polymer Materials," *International Journal of Adhesion and Adhesives*, **24**, 455–460 (2004).
36. Bruck, H.A., Fowler, G., Gupta, S.K., and Valentine, T.M., "Using Geometric Complexity to Enhance the Interfacial Strength of Heterogeneous Structures Fabricated in a Multi-stage, Multi-piece Molding Process," *EXPERIMENTAL MECHANICS*, **44**, 261–271 (2004).
37. Roychowdhury, S., Roy, Y., and Dodds, R.H. Jr, "Ductile Tearing in Thin Aluminum Panels: Experiments and Analyses Using Large-displacement, 3-D Surface Cohesive Elements," *Engineering Fracture Mechanics*, **69**, 983–1002 (2002).
38. Li, Z., Bi, X., Lambros, J., and Geubelle, P.H., "Dynamic Fiber Debonding and Frictional Push-out in Model Composite Systems: Experimental Observations," *EXPERIMENTAL MECHANICS*, **42**, 417–425 (2002).